ELECTRONIC RESEARCH ARCHIVE
Volume **29**, Number **5**, November **2021**

doi:10.3934/era.2021027
pp. **3081–3096**

SIMULTANEOUS RECOVERY OF SURFACE HEAT FLUX AND THICKNESS OF A SOLID STRUCTURE BY ULTRASONIC MEASUREMENTS

Youjun Deng[1], Hongyu Liu[2,*], Xianchao Wang[2]
Dong Wei[3,4] and Liyan Zhu[1]

[1]School of Mathematics and Statistics, HNP-LAMA, Central South University
Changsha, Hunan 410083, China
[2]Department of Mathematics, City University of Hong Kong
Kowloon, Hong Kong, China
[3]State Key Laboratory of Aerodynamics
China Aerodynamics Research and Development Center
Mianyang, Sichuan 621000, China
[4]Center of Nondestructive Examination
China Special Equipment Inspection and Research Institute
Beijing 100029, China

Abstract. This paper is concerned with a practical inverse problem of simultaneously reconstructing the surface heat flux and the thickness of a solid structure from the associated ultrasonic measurements. In a thermoacoustic coupling model, the thermal boundary condition and the thickness of a solid structure are both unknown, while the measurements of the propagation time by ultrasonic sensors are given. We reformulate the inverse problem as a PDE-constrained optimization problem by constructing a proper objective functional. We then develop an alternating iteration scheme which combines the conjugate gradient method and the deepest decent method to solve the optimization problem. Rigorous convergence analysis is provided for the proposed numerical scheme. By using experimental real data from the lab, we conduct extensive numerical experiments to verify several promising features of the newly developed method.

1. **Introduction.** The heat conduction is a ubiquitous phenomenon which forms the basis for many practical applications. Given the geometrical and material configurations of a material structure as well as the heat source including the initial and boundary temperature distributions, finding the temperature distribution as well as its change on the material structure constitutes the so-called direct or forward heat conduction problem. In many practical applications, one is more interested in the so-called inverse heat conduction problem which reverses the above forward problem through direct or indirect measurement data; see e.g. [1, 13, 14, 20, 24] and the references cited therein for some related studies in the literature.

In this paper, motivated by practical applications (with experimental real data from the lab), we are mainly concerned with the reconstruction of the surface heat

2020 *Mathematics Subject Classification.* Primary: 35K05, 49N45, 65N21.
Key words and phrases. Thermoacoustic coupling, inverse problem, heat flux and thickness, ultrasonic measurements, adjoint state method, convergence analysis.
* Corresponding author: Hongyu Liu.

flux and the thickness of a solid structure by using the associated ultrasonic measurements. The reconstruction of the surface heat flux is one of the most typical inverse heat conduction problems, and is widely encountered in aerospace, nuclear physics, metallurgy, and other industrial fields; see [14] and the references cited therein for more related discussions. Ultrasonic thickness measurement is a commonly used non-destructive testing method, and is widely used in petroleum, machinery, ship, chemical industry and other fields [20]. For most of existing results in the literature, one either recovers the surface heat flux by assuming the thickness of the material structure is a priori known, or recovers the thickness of the material structure by assuming the surface heat flux is a priori known. However, it is a more practical scenario that both the surface heat flux and the thickness of the material structure are unknown and one recovers both of them.

In this paper, based on the ultrasonic echo method and the inverse analysis method of the heat conduction, we propose a novel scheme for simultaneously recovering the surface heat flux and the thickness of the material structure through the pulse-echo measurements by the ultrasonic probe. The study is posed as an inverse problem associated with a thermoacoustic coupling model. We recast the inverse problem as a PDE (partial differential equation)-constrained optimization problem by constructing a proper objective functional. We then develop an alternating iteration scheme which combines the conjugate gradient method and the deepest decent method to solve the optimization problem. Rigours convergence analysis is provided for the proposed numerical scheme. Finally, by using experimental real data from the lab, we conduct extensive numerical experiments to verify effectiveness and efficiency of the method.

The rest of this paper is organized as follows. In Section 2, we present the mathematical formulation of the direct and inverse problems for our study and also briefly discuss the corresponding physical setup. In Section 3, we give the optimization formulation of the inverse problem and then derive the alternating iteration scheme for solving the optimization problem. Sections 4 and 5 are, respectively, devoted to the theoretical convergence analysis and numerical experiments.

2. **Mathematical and physical setups.** The physical principle of the ultrasonic thickness measurement is to use the propagation time of the ultrasonic waves in the medium to infer the thickness of the underlying solid structure. The propagation time is mainly determined by the thickness, material properties, and internal temperature field of the solid structure; see Figure 1 for a schematic illustration of the physical setup. The propagation time of the ultrasonic wave in the solid structure can be expressed as (see [23]):

$$\Lambda_L(t) = 2\int_0^L \frac{1}{V(T(x,t))}\,\mathrm{d}x, \quad t \in (0,+\infty), \tag{2.1}$$

where $L \in \mathbb{R}_+$ denotes the unidirectional propagation distance of the ultrasonic wave in the medium, i.e. the thickness of the material structure being under detection. Here, V is the propagation velocity of the acoustic wave in the solid medium and is related to the material properties and the structure temperature. Usually, it has an approximately linear relationship with the temperature, i.e.,

$$V(T) = aT + b, \quad a,\, b \in \mathbb{R}, \tag{2.2}$$

where a and b are determined by the properties of the material and calibrated by experiments. $T(x,t)$ is the internal temperature of the structure, which satisfies the

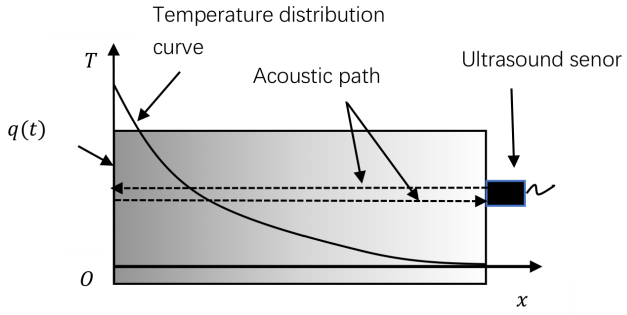

FIGURE 1. A one-dimensional model based on ultrasonic detection.

following heat conduction system for $T \in W_2^{2,1}([0,L]\times(0,\tau))$:

$$\begin{cases} \rho c\dfrac{\partial T}{\partial t} = \dfrac{\partial}{\partial x}\left(k\dfrac{\partial T}{\partial x}\right), & (x,t)\in[0,L]\times[0,\tau], \\ -k\dfrac{\partial T}{\partial x}\Big|_{x=0} = q, \quad -k\dfrac{\partial T}{\partial x}\Big|_{x=L} = 0, & q(t)\in L^2[0,\tau], \\ T\,|_{t=0} = T_0, & x\in[0,L], \end{cases} \tag{2.3}$$

where $k(x)$, $c(x)$ and $\rho(x)$ are the thermal conductivity, specific heat capacity and density of the material, respectively, and $q(t)$ denotes the heat flux density on the boundary. In this paper, the parameters k, c, ρ are set to constants, which is in accordance with the lab experiments, see the numerical part in Section 5.

In this paper, the inverse problem that we are concerned with is described as follows:

Problem 1. *Given the measured propagation time of the ultrasonic wave $\Lambda_m(t)$ and the measured boundary temperature $T_m(L,t)$, determine the surface heat flux $q(t)$ and the thickness L, i.e.,*

$$\{\Lambda_m(t), T_m(L,t)\} \to \{q(t), L\}, \quad t\in[0,\tau]. \tag{2.4}$$

We would like to point out that in the measured data, the temperature at the end of the solid structure can be measured. However the thickness L of the structure is unknown in the practical application of our interest. It can be directly verified that the inverse problem (2.4) is nonlinear.

3. An alternating iteration scheme for the inverse problem.

In this section, we first recast the inverse problem (2.4) as an optimization problem by following the general framework of Tikhonov regularization for inverse problems; see e.g. [9] and the references cited therein. Then we present the newly proposed alternating iteration scheme. To that end, we introduce the following objective functional with respect to the unknown heat flux $q(t)$ and thickness L:

$$J(q,L) = \frac{1}{2}\int_0^\tau (\Lambda_L(t) - \Lambda_m(t))^2\,\mathrm{d}t + \frac{\alpha}{2}\int_0^\tau (T(L,t) - T_m(L,t))^2\,\mathrm{d}t, \tag{3.1}$$

where $\alpha \in \mathbb{R}_+$ signifies a regularization parameter. We then recast the inverse problem (2.4) as the following PDE-constrained optimization problem:

$$\min_{q\in L^2(0,\tau),\, L\in\mathbb{R}_+} J(q,L) \quad \text{subject to } T \in W_2^{2,1}([0,L]\times(0,\tau)) \text{ satisfying } \quad (2.3). \tag{3.2}$$

We next convert the constrained optimization problem into an unconstrained one by using the Lagrange multiplier method. Using the heat conduction equation (2.3), with the boundary conditions and the initial condition, the augmented functional is given as follows:

$$\begin{aligned} J(q,L) =& \frac{1}{2}\int_0^\tau \left(\Lambda_L(t)-\Lambda_m(t)\right)^2 \mathrm{d}t + \frac{\alpha}{2}\int_0^\tau \left(T(L,t)-T_m(L,t)\right)^2 \mathrm{d}t \\ &- \int_0^L\int_0^\tau \left\{\rho c\frac{\partial T(x,t)}{\partial t} - \frac{\partial}{\partial x}\left(k\frac{\partial T(x,t)}{\partial x}\right)\right\}\lambda_1(x,t)\,\mathrm{d}t\mathrm{d}x \\ &+ \int_0^\tau \left(k\frac{\partial T(x,t)}{\partial x}+q(t)\right)\Big|_{x=0}\lambda_2(t)\,\mathrm{d}t + \int_0^\tau \left(k\frac{\partial T(x,t)}{\partial x}\right)\Big|_{x=L}\lambda_3(t)\,\mathrm{d}t \\ &- \int_0^L \left(T(x,t)-T_0(x,t)\right)\Big|_{t=0}\lambda_4(x)\,\mathrm{d}x. \end{aligned} \tag{3.3}$$

where $\lambda_1(x,t)$, $\lambda_2(t)$, $\lambda_3(t)$ and $\lambda_4(x)$ denote the Lagrange multipliers.

3.1. **Gradients with respect to the parameters.** To solve the optimization problem (3.3), the gradients of the objective functional J with respective to q and L are required. However, it is difficult to solve the gradients directly. Thus, we refer to [19] and use the adjoint state method to derive them. Noting that

$$\begin{aligned} &\int_0^L\int_0^\tau \rho c\frac{\partial T(x,t)}{\partial t}\lambda_1(x,t)\,\mathrm{d}t\mathrm{d}x \\ &= -\int_0^L\int_0^\tau \rho c\frac{\partial \lambda_1(x,t)}{\partial t}T(x,t)\,\mathrm{d}t\mathrm{d}x + \int_0^L \left(\rho c\lambda_1(x,t)T(x,t)\right)\Big|_0^\tau \mathrm{d}x. \end{aligned}$$

Similarly, one can deduce that

$$\begin{aligned} \int_0^L\int_0^\tau \frac{\partial}{\partial x}\left(k\frac{\partial T(x,t)}{\partial x}\right)\lambda_1(x,t)\,\mathrm{d}t\mathrm{d}x =& \int_0^L\int_0^\tau \frac{\partial}{\partial x}\left(k\frac{\partial \lambda_1(x,t)}{\partial x}\right)T(x,t)\,\mathrm{d}t\mathrm{d}x \\ &+ \int_0^\tau \left(k\lambda_1(x,t)\frac{\partial T(x,t)}{\partial x}\right)\Big|_0^L \mathrm{d}t \quad - \int_0^\tau \left(k\frac{\partial \lambda_1(x,t)}{\partial x}T(x,t)\right)\Big|_0^L \mathrm{d}t. \end{aligned}$$

Finally, the equation (3.3) can be rewritten as

$$\begin{aligned} J(q,L) =& \frac{1}{2}\int_0^\tau \left(\Lambda_L(t)-\Lambda_m(t)\right)^2 \mathrm{d}t + \frac{\alpha}{2}\int_0^\tau \left(T(L,t)-T_m(L,t)\right)^2 \mathrm{d}t \\ &+ \int_0^L\int_0^\tau \left\{\rho c\frac{\partial \lambda_1(x,t)}{\partial t} + \frac{\partial}{\partial x}\left(k\frac{\partial \lambda_1(x,t)}{\partial x}\right)\right\}T(x,t)\,\mathrm{d}t\mathrm{d}x \\ &+ \int_0^\tau \left(k\lambda_1(x,t)\frac{\partial T(x,t)}{\partial x}\right)\Big|_0^L \mathrm{d}t - \int_0^\tau \left(k\frac{\partial \lambda_1(x,t)}{\partial x}T(x,t)\right)\Big|_0^L \mathrm{d}t \end{aligned}$$

$$-\int_0^L \left(\rho c\lambda_1(x,t)T(x,t)\right)\Big|_0^\tau \mathrm{d}x + \int_0^\tau \left(k\frac{\partial T(x,t)}{\partial x} + q(t)\right)\Big|_{x=0} \lambda_2(t)\,\mathrm{d}t$$
$$+\int_0^\tau \left(k\frac{\partial T(x,t)}{\partial x}\right)\Big|_{x=L} \lambda_3(t)\,\mathrm{d}t - \int_0^L \left(T(x,t)-T_0(x,t)\right)\Big|_{t=0} \lambda_4(x)\,\mathrm{d}x.$$

To obtain the adjoint state equation, we set

$$\frac{\partial J}{\partial T} = 0,$$

and it yields

$$\begin{cases} \rho c\dfrac{\partial \lambda_1(x,t)}{\partial t} + \dfrac{\partial}{\partial x}\left(k\dfrac{\partial \lambda_1(x,t)}{\partial x}\right) = S(x,t), \\ -k\dfrac{\partial \lambda_1(x,t)}{\partial x}\Big|_{x=0} = 0, \quad -k\dfrac{\partial \lambda_1(x,t)}{\partial x}\Big|_{x=L} = 0, \\ \lambda_1(x,\tau) = 0, \\ \lambda_2(t) = \lambda_1(0,t), \\ \lambda_3(t) = -\lambda_1(L,t), \\ \lambda_4(x) = -\rho c\lambda_1(x,0). \end{cases}$$

Here the source term is given by

$$S(x,t) = 2\left(\Lambda_L(t) - \Lambda_m(t)\right)\frac{a}{(V(x,t))^2} + \frac{\alpha}{L}\left(T(L,t) - T_m(L,t)\right).$$

From (3.3), through a straightforward calculation, the gradients with respect to the model parameters are given by

$$\begin{cases} \dfrac{\partial J}{\partial q}(t) = \lambda_2(t) = \lambda_1(0,t), \\ \dfrac{\partial J}{\partial L} = \displaystyle\int_0^\tau \left(\Lambda_L(t) - \Lambda_m(t)\right)\frac{\partial \Lambda_L(t)}{\partial L}\,\mathrm{d}t = \int_0^\tau \frac{2\left(\Lambda_L(t) - \Lambda_m(t)\right)}{V(L,t)}\,\mathrm{d}t. \end{cases} \tag{3.4}$$

In order to change the final condition to initial condition, a change of variables can be employed :

$$\mu(x,t) = \lambda_1(x,\tau - t).$$

Consequently, the adjoint state equation is rewritten as

$$\begin{cases} \rho c\dfrac{\partial \mu(x,t)}{\partial t} + \dfrac{\partial}{\partial x}\left(k\dfrac{\partial \mu(x,t)}{\partial x}\right) = S(x,\tau - t), \\ -k\dfrac{\partial \mu(x,t)}{\partial x}\Big|_{x=0} = 0, \quad -k\dfrac{\partial \mu(x,t)}{\partial x}\Big|_{x=L} = 0, \\ \mu(x,0) = 0. \end{cases}$$

Therefore, according to (3.4), the gradients with respect to $q(t)$ and L can be represented by

$$\begin{cases} \dfrac{\partial J}{\partial q}(t) = \lambda_1(0,t) = \mu(0,\tau - t), \\ \dfrac{\partial J}{\partial L} = \displaystyle\int_0^\tau \left(\Lambda_L(t) - \Lambda_m(t)\right)\frac{\partial \Lambda(t)}{\partial L}\,\mathrm{d}t = \int_0^\tau \frac{2\left(\Lambda_L(t) - \Lambda_m(t)\right)}{V(L,t)}\,\mathrm{d}t. \end{cases}$$

Next, we use the conjugate gradient method and the steepest descent method to identify the heat flux $q(t)$ and the thickness L, respectively.

3.2. **Update q with the conjugate gradient method.** To numerically reconstruct the heat flux q, we shall discretize the heat flux with respect to the time t. Suppose that $[0,\tau]$ is discretized as follows

$$0 = t_0 \le t_1 \le \cdots \le t_i \le t_{i+1} \le \cdots \le t_N = \tau.$$

The reconstruction schemes of the heat flux based on the conjugate gradient (CG) method is described as follows

$$q_i^{n+1} = q_i^n + \beta^n p_i^n, \tag{3.5}$$

where the subscript i indicates the discretization of the heat flux in time, and the superscripts n and $n+1$ denote the iteration steps. p_i^n signifies the conjugate direction and it is generated by the rule

$$p_i^n = \begin{cases} -g_i^n, & n = 1, \\ -g_i^n + \alpha^n p_i^{n-1}, & n \ge 2, \end{cases}$$

where α^n is the CG update parameter given by

$$\alpha^n = \frac{\sum_{i=0}^{N} (g_i^n)^T (g_i^n - g_i^{n-1})}{\sum_{i=0}^{N} \left\| g_i^{n-1} \right\|^2},$$

with $\|\cdot\|$ denoting the Euclidean norm, and

$$g_i^n = \frac{\partial J}{\partial q}\Big|_{t=t_i}^n.$$

In addition, the step size β^n is obtained by the exact line search and can be described as

$$\beta^n = \frac{\sum_{i=0}^{N} \left(\Lambda_L^n(t_i) - \Lambda_m(t_i)\right) \Delta t_{in}}{\sum_{i=0}^{N} \left[\Delta t_{in}\right]^2},$$

where $\Lambda_L^n(t)$ is the solution of the forward problem and Δt_n is the change in transmission time and can be expressed as:

$$\Delta t_n(t) = \int_0^L \frac{1}{V_{g^n}(x,t)} \mathrm{d}x.$$

Here $V_{g^n} = aT_{g^n} + b$ and $T_{g^n}(x,t)$ is the solution of the following sensitivity equation

$$\begin{cases} \rho c \dfrac{\partial T}{\partial t} = \dfrac{\partial}{\partial x}\left(k \dfrac{\partial T}{\partial x}\right), \\ -k \dfrac{\partial T}{\partial x}\Big|_{x=0} = g^n, \quad -k \dfrac{\partial T}{\partial x}\Big|_{x=L} = 0, \\ T|_{t=0} = T_0. \end{cases}$$

3.3. **Update L with the steepest descent method.** The reconstruction of the thickness based on the steepest descent method is described as follows:

$$L^{n+1} = L^n + \lambda^n d^n, \tag{3.6}$$

where the superscripts n and $n+1$ denote the iteration steps, and d^n denotes the negative gradient direction respect to L,

$$d^n = -\frac{\partial J}{\partial L}\bigg|_{L=L^n} = \int_0^\tau \frac{2\left(\Lambda_m(t) - \Lambda_L(t)\right)}{V(L^n, t)}\,\mathrm{d}t.$$

And the step size λ^n is determined by an inexact line search technique called Wolfe-Powell search method. Assuming that $f(L) = J(q, L)$ is differentiable, the Wolfe-Powell search method is used to find λ^n along d^n such that

$$\nabla f(L^n + \lambda^n d^n)^T d^n \geq \sigma \nabla f(L^n)^T d^n,$$

$$f(L^n + \lambda^n d^n) \leq f(L^n) + \rho \nabla f(L^n)^T d^n, \quad \rho \in (0, 1/2), \sigma \in (\rho, 1).$$

Assuming that $\varphi(\lambda^n) = f(L^n + \lambda^n d^n)$, the strategy for computing the step length λ^n can be described as follows:

Step1. Let $\lambda^0 = 0, \lambda^{max} > 0$, and choose $\lambda^1 \in [\lambda^0, \lambda^{max}], \rho \in (0, 1/2), \sigma \in (\rho, 1)$. Evaluate $\varphi(\lambda^0)$ and $\varphi^{'}(\lambda^0)$. Let $a_0 = \lambda^0, b_0 = \lambda^{max}, n = 0$.

Step2. Evaluate $\varphi(\lambda^n)$. If $\varphi(\lambda^n) \leq \varphi(\lambda^0) + \rho\lambda^n\varphi^{'}(\lambda^0)$, go to **Step3**. Else, go to **Step4**, set $a_{n+1} = a_n, b_{n+1} = \lambda^n$.

Step3. Evaluate $\varphi^{'}(\lambda^n)$. If $\varphi^{'}(\lambda^n) \geq \sigma\varphi^{'}(\lambda^0)$, stop. Else, set $a_{n+1} = \lambda^n, b_{n+1} = b_n$, go to **Step4**.

Step4. Let $\lambda^{n+1} = \dfrac{a_{n+1} + b_{n+1}}{2}$, set $n = n + 1$, go to **Step2**.

3.4. **Optimize algorithm iteration format.** In this paper, we iterate the heat flux q and the thickness L alternatively, and the proposed algorithm is listed as follows:

Step1. Choose an initial point q_i^0, L^0, $\varepsilon \in (0, 1)$.

Step2. Fixed L^n. Update q_i using the formular (3.5).

Step3. Fixed q_i^{n+1} update L using the formular (3.6).

Step4. Evaluate $J(q_i^{n+1}, L^{n+1})$. If $J(q_i^{n+1}, L^{n+1}) < \varepsilon$, stop. Else, set $n = n + 1$, go to **Step2**.

4. **Convergence analysis.** In this section, we shall analyze the convergence of the reconstruction scheme proposed in the previous section. In recent decades, convergence analysis of strongly convex functionals for inverse problems has attracted a lot of interest and related therein has been studied. Klibanov *et al*[15, 16] proposed a convexification method via constructing a globally strictly convex functionals for the inverse coefficient problems. We also refer the readers to [2] and the references algorithms for constructing weighted globally strictly convex cost functionals by the Carleman estimates.

Let (q_i^*, L^*) be the optimal solution to the optimization problem (3.3), i.e.,

$$J\left(q_i^*, L^*\right) \leq J\left(q_i^n, L^n\right), \quad \forall\, q_i^n \in \mathbb{R}^N,\ L^n \in \mathbb{R}. \tag{4.1}$$

It is clear that the necessary condition of (4.1) is:

$$\nabla J\left(q_i^*, L^*\right) = \left(g_i^*, -d^*\right)^T = 0,$$

Algorithm 1 Alternating iteration algorithm

Require: $q^0(N), L^0, crl, n_{max}, \varepsilon$.
Ensure: $q(N)$, L, $T(nl)$.
$q^n \leftarrow q^0$, $L^n \leftarrow L^0$, $J \leftarrow J^0$.
while $abs(J) > crl.AND.n < n_{max}$ **do**
  call gradient
  $g^n \leftarrow g1$,
  call cgm
  $p^n \leftarrow p1$,
  call bet
  $\beta^n \leftarrow \beta 1$,
  for $i = 1, N$ **do**
    $q^n(i) \leftarrow q^n(i) - bet * p^n(i)$
    $g2(i) \leftarrow g1(i)$
    $p2(i) \leftarrow p1(i)$
  end for
  // update q
  if $abs(L - j1) > \varepsilon$ **then**
    $j1 \leftarrow L$
    call wolfe(j)
    // update L
  else
    $aa \leftarrow aa/10$
    // update regularization parameter
  end if
  compute objective function J.
end while

and hence it is sufficient for us to prove

$$\lim_{n\to\infty} \inf \| (g_i^n, d^n) \| = 0. \tag{4.2}$$

Next, we prove that the optimization algorithm that consists of (3.5) and (3.6) satisfies the convergence condition (4.2). Before we discuss the convergence, we introduce some notations and important lemmas.

Definition 4.1. $Polka - Ribiére - Polyak(PRP)$ method is a nonlinear conjugate gradient method, and it has the following form:

$$\begin{aligned} q^{n+1} &= q^n + \beta^n p^n, \\ p^n &= \begin{cases} -g^n, & n = 1, \\ -g^n + \alpha^n p^{n-1}, & n \geq 2, \end{cases} \end{aligned} \tag{4.3}$$

where

$$\alpha_{PRP}^n = \frac{g^{nT}(g^n - g^{n-1})}{\|g^{n-1}\|^2}. \tag{4.4}$$

Definition 4.2. Exact line search: at each iteration, the step size β^n is selected so that

$$f(q^n + \beta^n p^n) = \min_{\beta} f(q^n + \beta p^n),$$

where the objective functional is $f(q) = J(q, L), q(t) \in L^2([0, \tau])$.

Remark 4.1. Iteration algorithm (3.5) is a PRP conjugate method with the exact line search.

Next, we prove the convergence of the PRP conjugate method with an exact line search as well as its convergence condition. To that end, we first derive several auxiliary lemmas.

Lemma 4.1. [21] *Let θ_n be the angle between the searching direction p^n and the negative gradient direction $-g^n$. Then*

$$\cos\theta_n = \frac{-g^{nT}p^n}{\|g^n\|\|p^n\|}.$$

When the line search is the exact line search, the angle θ_n is represented by Figure 2. If α is given by (4.4), we have

$$\tan\theta_{n+1} \le \sec\theta_n \frac{\|g^{n+1} - g^n\|}{\|g^n\|}. \tag{4.5}$$

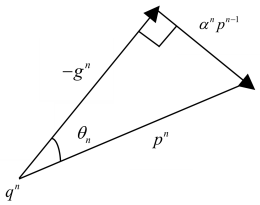

FIGURE 2. The definition of figure

Proof. Figure 2 gives the equation

$$\|p^n\| = \sec\theta_n \|g^n\|. \tag{4.6}$$

Further, if n is replaced by $n+1$ in Figure 2 , we find the identity

$$\alpha^{n+1}\|p^n\| = \tan\theta_{n+1}\|g^{n+1}\|. \tag{4.7}$$

By (4.4), one has

$$\alpha^{n+1} = \frac{(g^{n+1})^T(g^{n+1} - g^n)}{\|g^n\|^2},$$

and hence by the Cauchy-Schwarz inequality,

$$\alpha^{n+1} \le \frac{\|g^{n+1}\|\,\|g^{n+1} - g^n\|}{\|g^n\|^2}. \tag{4.8}$$

Next, by the elimination of $\|g^n\|$ from (4.6) and(4.7), one can show the following equality,

$$\alpha^{n+1} = \frac{\tan\theta_{n+1}\|g^{n+1}\|}{\sec\theta_n\|g^n\|}, \tag{4.9}$$

which in combination with (4.8) and (4.9) readily yields that

$$\tan\theta_{n+1} \le \sec\theta_n \frac{\|g^{n+1} - g^n\|}{\|g^n\|}.$$

The proof is complete. □

Lemma 4.2. [6] *Consider the iterative method of the form* $q^{n+1} = q^n + \beta^n p^n$, *where* p^n *satisfies the descent condtion* $p^{nT} g^n \leq 0$, *the step size* β^n *is obtained by the exact line search, the objective functional* $f(q)$ *is bounded below, and its gradient* $\nabla f(q)$ *satisfies the Lipschitz condition, then*

$$\sum_{n\geq 1} \frac{(g^{nT} p^n)^2}{\|p^n\|^2} < \infty, \tag{4.10}$$

and according to the definition of θ_n, (4.10) *is equivalent to*

$$\sum_{n\geq 1} \|g^n\|^2 \cos\theta_n < \infty. \tag{4.11}$$

Lemma 4.3. [25] *If the step size* β^n *is obtained by the exact line search and the objective function* $f(q)$ *is uniformly convex, then*

$$f(q^n) - f(q^n + s^n) \geq c\,\|s^n\|^2$$

holds, where $s^n = q^{n+1} - q^n$, $c > 0$ *is a constant, and further there is* $\|s^n\| \to 0$ *as* $n \to \infty$.

Lemma 4.4. *Assume that the objective function* $f(q)$ *is uniformly convex and bounded from below, and its gradient* $\nabla f(q)$ *satisfies the Lipschitz condition. Consider the algorithm* (4.3)–(4.4), *if the step size* β^n *is obtained by the exact line search, then*

$$\lim_{n\to\infty} \inf \|g^n\| = 0.$$

Proof. The proof follows a similar spirit to that of Theorem 1 in [21]. By an absurdity argument, we assume that the theorem does not hold. Then there is a constant γ, such that for any $n \geq 1$,

$$\|g^n\| \geq \gamma. \tag{4.12}$$

By Lemma 4.3, there is $\|s^n\| \to 0, n \to \infty$, which combines with the fact that $\nabla f(q)$ is Lipschitz continuous implies that there exists a positive integer m, such that

$$\left\|g^{n+1} - g^n\right\| \geq \frac{1}{2}\gamma, \tag{4.13}$$

which holds for any $n \geq m$. Noticing that for any $\theta_n \in [0, \pi/2)$, there is

$$\sec\theta_n \leq 1 + \tan\theta_n,$$

which together with (4.5), (4.12) and (4.13) further implies that

$$\tan\theta_{n+1} \leq \frac{1}{2} + \frac{1}{4} + \cdots + (\frac{1}{2})^{n-1-m}(1 + \tan\theta_m) \quad = 1 + \tan\theta_m, \quad \forall n \geq m.$$

Therefore, the angle θ_n between the searching direction p_n and the negative gradient direction $-g^n$ is always smaller than an angle bounded above by $\pi/2$. Therefore, by (4.11), we have $\|g^n\| \to 0$, which is a contradiction to (4.12). Thus the theorem must hold true.

The proof is complete. □

Next, we establish the convergence of the steepest descent algorithm with the Wolfe-Powell step search method.

Lemma 4.5. [22] *Let the objective function $f(L) = J(q, L), L \in \mathbb{R}$ be differentiable and bounded from below, and $g(L) = \nabla f(L)$ satisfy the Lipschitz condition. Suppose that the steepest descent method generates a sequence $L^n, n \geq 1$, using the recurrence*

$$L^{n+1} = L^n + \lambda^n d^n,$$

where the direction d^n denotes the negative gradient direction. If the step size λ satisfies

$$\begin{cases} (g^{n+1})^T d^n \geq \sigma (g^n)^T d^n, \\ f(L^{n+1}) \leq f(L^n) - \rho \lambda^n (d^n)^2, \quad \rho \in (0, 1/2), \sigma \in (\rho, 1), \end{cases}$$

where $g^{n+1} = g(L^{n+1}) = g(L^n + \lambda^n d^n)$, then one has

$$f(L^n) - f(L^{n+1}) \geq \frac{\rho(1-\sigma)}{M} \|g^n\|^2 \cos^2 \theta_n.$$

Lemma 4.6. *If the function $f(L)$ is continuously differentiable and satisfys the conditions of Lemma 4.5, then sequence L^n generated by the steepest descent method satisfys:*

$$\lim_{n \to \infty} \|g^n\|^2 = 0.$$

Proof. By Lemma 4.5,

$$f(L^n) - f(L^{n+1}) \geq \frac{\rho(1-\sigma)}{M} \|g^n\|^2 \cos^2 \theta_n.$$

Thus

$$\begin{aligned} f(L^0) - f(L^{n+1}) &= [f(L^0 - f(L^1)] + [f(L^1) + f(L^2)] + \cdots + [f(L^n) - f(L^{n+1})] \\ &= \sum_{k=0}^{n} [f(L^k) - f(L^{k+1})] \geq \sum_{k=0}^{n} \frac{\rho(1-\sigma)}{M} \|g^k\|^2 \cos^2(d^k, -g^k). \end{aligned} \tag{4.14}$$

Notice that $\cos^2(d_k, -g_k) = 1, k = 1, 2, \cdots, n$. We therefore have from (4.14) that

$$\sum_{k=0}^{n} \frac{\rho(1-\sigma)}{M} \|g_k\|^2 \leq f(L^0) - f(L^{n+1}). \tag{4.15}$$

Since $f(L)$ is bounded from below, one sees that $f(L^0) - f(L^{n+1}) < \infty$, which together with (4.15) readily implies that

$$\lim_{n \to \infty} \|g^n\|^2 = 0.$$

The proof is complete. □

Next we prove that the optimization algorithm consisting of (3.5) and (3.6) satisfies the convergence condition (4.2).

Theorem 4.1. *Consider the iterative algorithm consisting of (3.5) and (3.6):*

$$\begin{cases} q_i^{n+1} = q_i^n + \beta^n p_i^n, \\ L^{n+1} = L^n + \lambda^n d^n, \end{cases}$$

Assume that the objective functional $J(q, L)$ satisfies the following conditions:
(a): $J(q, L)$ is continuously differentiable with respect to $q(t)$ and L;
(b): $J(q, L)$ is uniformly convex;
(c): $J(q, L)$ is bounded from below;
(d): Its gradient $\nabla J(q, L)$ is Lipschitz continuous.

Then the optimization algorithm consisting of (3.5) *and* (3.6) *satisfies the convergence condition* (4.2)*, i.e.,*

$$\liminf_{n\to\infty} \| (g_i^n, d^n) \|_1 = 0,$$

where $\|\cdot\|_1$ *denotes the* l^1*-norm, namely* $\| (g_i^n, d^n) \|_1 = \|g_i^n\|_1 + |d^n|$.

Proof. We first consider the iterative algorithm (3.5). Since the step size λ^n is searched by the Powell-Wolfe method, it satisfies the following conditions:

$$\begin{aligned} &\varphi(\lambda^n) \le \varphi(0) + \rho\lambda^n \varphi^{'}(0), \\ &\varphi^{'}(\lambda^n) \ge \sigma\varphi^{'}(0), \quad \rho \in (0, 1/2), \sigma \in (\rho, 1), \end{aligned} \tag{4.16}$$

where $\varphi(\lambda^n) = J(q^n, L^n + \lambda^n d^n)$. By using conditions (a) (c) (d) and (4.16), we see that Lemma 4.6 holds. Hence by Lemma 4.6, we have

$$\lim_{n\to\infty} |d^n| = 0. \tag{4.17}$$

We proceed to consider the iterative algorithm (3.6). By virtue of the conditions (a) (b) (c) (d), we see that the iteration algorithm (3.5) is a PRP conjugate method with the exact line search. By Lemma 4.4,

$$\lim_{n\to\infty} \inf \|g_i^n\| = 0, \tag{4.18}$$

According to (4.17) and (4.18),

$$\lim_{n\to\infty} \inf (\|g_i^n\| + |d^n|) = 0.$$

Thus,

$$\lim_{n\to\infty} \inf \| (g_i^n, d^n) \|_1 = \lim_{n\to\infty} \inf (\|g_i^n\| + |d^n|) = 0.$$

The proof is complete. □

5. **Numerical examples.** In this section, we present several numerical examples to verify the effectiveness and robustness of the proposed scheme in simultaneously reconstructing the surface heat flux and the thickness of a solid structure under different acoustic time accuracies, initial fluxes, and initial thicknesses. It is emphasized that all the data in our numerical examples are collected by lab experiments following the setup described in Figure 1. In fact , these measured data are blind data without any priori information and we didn't make any preprocessing for these data.

The specimens with a thickness of $L = 50\,\text{mm}$ are heated at one boundary and the surface heat flux is $q(t) = 10^5\,\text{J/s}$. The ultrasonic wave probes are stalled on the other boundary of the specimens with the detection frequency set to be $\omega = 1\,\text{Hz}$, and the total detection time set to be $\tau = 500\,\text{s}$. Moreover, the thermal conductivity of the specimens is $k = 50\,\text{W/(m}\cdot{}^\circ\text{C)}$, specific heat is $c = 400\,\text{J/(kg}\cdot{}^\circ\text{C)}$ and density of the material is $\rho = 7800\,\text{kg/m}^3$. The initial tempareture is chosen as $T_0 = 26\,^\circ\text{C}$. The relationship between the velocity and temperature is given as follows:

$$V(T) = -0.4521T + 3259.9.$$

In the following numerical examples, the stopping criterion for the iterations is set to be $J(q, L) < 5 \times 10^{-18}$. The Fortran software is used for implementing of Algorithm 1.

The reconstruction results of thickness under the acoustic time accuracy of 10^{-9}, 10^{-10} and 10^{-11} are respectively shown in the Table 1.

Acoustic time accuracy (s)	initial heat flux q^0(J/s)	initial thickness L^0(mm)	reconstructed thickness L(mm)	iterations n
10^{-9}	0	3	50.0006	138
10^{-10}	0	3	50.0006	64
10^{-11}	0	3	50.0006	63
10^{-9}	1×10^3	45	50.0032	208
10^{-10}	1×10^3	45	50.0028	115
10^{-11}	1×10^3	45	50.0025	108

TABLE 1. Convergence of the iteration method with different initial guesses and measurement errors.

It can be found that the thickness can be reconstructed effectively under different acoustics time accuracies. The error and the number of iterations show that under the same initial value, the accuracy of acoustic time will affect the convergence speed of the algorithm. If the accuracy of acoustic time reaches 10^{-10} or 10^{-11}, one can achieve much accurate reconstruction results. Thus, in the following numerical examples, we adopt the measurement data with an acoustic time accuracy of 10^{-10} or 10^{-11} to study the effect of the initial values on the inversion procedure.

Figure 3 presents the reconstruction results of the heat flux under different initial thicknesses and different initial heat flux conditions. The acoustic accuracy is fixed to be 10^{-10}.

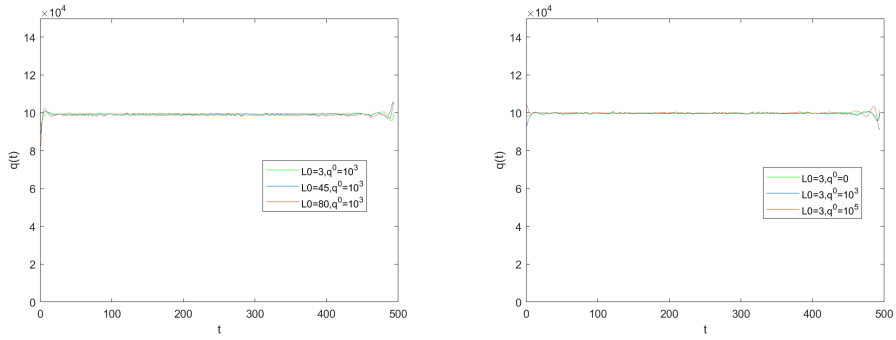

(a) (b)

FIGURE 3. Heat flux inversion results with the acoustic time accuracy fixed to be 10^{-10}. (a): under a fixed initial heat flux and different initial thicknesses, (b): under a fixed initial thickness and different initial heat fluxes.

Figure 4 shows the reconstruction results of the heat flux under different initial thicknesses and different initial heat flux conditions. The acoustic accuracy is fixed to be 10^{-11}.

By observing the surface heat flux reconstruction results in Figures 3 and 4, it can be found that when the acoustic time accuracy is 10^{-10} and 10^{-11}, under different initial conditions, the inversion value of the heat flux converges to the real value. Moreover, when the acoustic time accuracy reaches 10^{-11}, the inversion

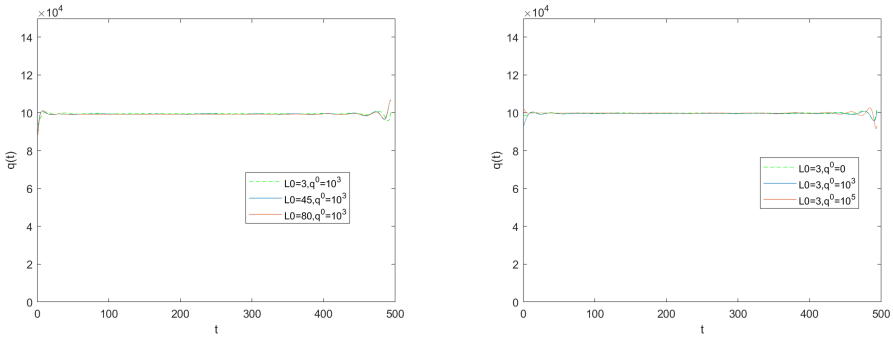

(a) (b)

FIGURE 4. Heat flux inversion results with the acoustic time accuracy fixed to be 10^{-11}. (a): under a fixed initial heat flux and different initial thicknesses, (b): under a fixed initial thickness and different initial heat fluxes.

value of heat flux very close to the real value, which achieves a much accurate reconstruction.

Table 2 lists the inversion results and the iteration times of the thickness under different initial thicknesses and different initial heat fluxes initial conditions. The acoustic time accuracy is 10^{-10} or 10^{-11}.

acoustic time accuracy	initial heat flux q^0(J/s)	initial thickness L^0(mm)	reconstructed thickness L(mm)	iterations n
10^{-10}	0	3	50.0006	64
10^{-10}	1×10^3	3	50.0016	58
10^{-10}	1×10^5	3	50.0000	133
10^{-10}	0	45	50.0025	126
10^{-10}	1×10^3	45	50.0028	115
10^{-10}	0	80	50.0028	77
10^{-10}	1×10^3	80	50.0046	92
10^{-11}	0	3	50.0006	63
10^{-11}	1×10^3	3	50.0016	57
10^{-11}	1×10^5	3	50.0006	147
10^{-11}	0	45	50.0025	126
10^{-11}	1×10^3	45	50.0025	108
10^{-11}	0	80	50.0028	77
10^{-11}	1×10^3	80	50.0029	80

TABLE 2. Convergence of the proposed iteration method with different initial guesses and measurement errors.

The results show that the iterative algorithm converges very fast and robust with different initial conditions.

6. **Conclusion.** Based on the ultrasonic echo method and the inverse problem analysis method of the heat conduction, combined with the optimization model, a method of simultaneously reconstructing the thickness and the surface heat flux of a solid structure is established in this paper. This approach is non-destructive and

non-contact and it can be used to recover the surface heat flux and the wall thickness at the same time. It possesses a high engineering value. We provide a rigorous convergence analysis of the proposed numerical scheme. By using experimental lab data, we conducted extensive numerical experiments to verify the effectiveness and efficiency of the newly developed method. It is found that as long as the acoustic time accuracy reaches 10^{-10} or 10^{-11}, the proposed iteration method converges very fast and robust with respect to different initial guesses. The inverse problems of simultaneously recovering more than one target objects can find important applications in geomagnetic anomaly detections [7, 8, 11], medical imaging [3, 10, 12] as well as many other areas [4, 5, 17, 18]. We believe the numerical method developed in this paper can be an inspiring source for the relevant numerical studies for those inverse problems.

Acknowledgments. The work of Y. Deng was supported by NSF grant of China No. 11971487 and NSF grant of Hunan No. 2020JJ2038. The work of H Liu was supported by a startup fund from City University of Hong Kong and the Hong Kong RGC General Research Fund (projects 12301420, 12302919, 12301218). The work of X. Wang was supported by the Hong Kong Scholars Program grant and the NSFC grant (projects XJ2019005, 12001140, 11971133).

REFERENCES

[1] O. M. Alifaov, *Inverse Heat Transfer Problems*, Spriger-Verlag, Berlin, 1994.
[2] A. L. Bukhgeim and M. V. Klibanov, Uniqueness in the large of a class of multidimensional inverse problems, *Dokl. Akad. Nauk SSSR*, **260** (1981), 269–272.
[3] X. Cao, H. Diao and H. Liu, Determining a piecewise conductive medium body by a single far-field measurement, *CSIAM Transactions on Applied Mathematics,* **1** (2020), 740–765.
[4] X. Cao, Y.-H. Lin and H. Liu, Simultaneously recovering potentials and embedded obstacles for anisotropic fractional Schrödinger operators, *Inverse Probl. Imaging*, **13** (2019), 197–210.
[5] X. Cao and H. Liu, Determining a fractional Helmholtz system with unknown source and medium parameter, *Commun. Math. Sci.*, **17** (2019), 1861–1876.
[6] Y. H. Dai and Y. Yuan, A nonlinear conjugate gradient method with a strong global convergence property, *SIAM J. Optim.*, **10** (1999), 177–182.
[7] Y. Deng, J. Li and H. Liu, On identifying magnetized anomalies using geomagnetic monitoring, *Arch. Ration. Mech. Anal.*, **231** (2019), 153–187.
[8] Y. Deng, J. Li and H. Liu, On identifying magnetized anomalies using geomagnetic monitoring within a magnetohydrodynamic model, *Arch. Ration. Mech. Anal.*, **235** (2020), 691–721.
[9] Y. Deng and Z. Liu, Iteration methods on sideways parabolic equations, *Inverse Problems*, **25** (2009), 095004, 14 pp.
[10] Y. Deng, H. Liu and X. Liu, Recovery of an embedded obstacle and the surrounding medium for Maxwell's system, *J. Differential Equations*, **267** (2019), 2192–2209.
[11] Y. Deng, H. Liu and W.-Y. Tsui, Identifying variations of magnetic anomalies using geomagnetic monitoring, *Discrete Contin. Dyn. Syst.*, **40** (2020), 6411–6440.
[12] Y. Deng, H. Liu and G. Uhlmann, On an inverse boundary problem arising in brain imaging, *J. Differential Equations*, **267** (2019), 2471–2502.
[13] W. Hu, Y. Gu and C.-M. Fan, A meshless collocation scheme for inverse heat conduction problem in three-dimensional functionally graded materials, *Eng. Anal. Bound. Elem.*, **114** (2020), 1–7.
[14] M. A. Kant and P. R. von Rohr, Determination of surface heat flux distributions by using surface temperature measurements and applying inverse techniques, *International Journal of Heat and Mass Transfer*, **99** (2016), 1–9.
[15] V. A. Khoa, G. W. Bidney, M. V. Klibanov, Loc H. Nguyen, Lam H. Nguyen, A. J. Sullivan and V. N. Astratov, Convexification and experimental data for a 3D inverse scattering problem with the moving point source, *Inverse Problems*, **36** (2020), 085007, 34 pp.
[16] M. V. Klibanov, J. Li and W. Zhang, Convexification of electrical impedance tomography with restricted Dirichlet-to-Neumann map data, *Inverse Problems,* **35** (2019), 035005, 33 pp.

[17] J. Li, H. Liu and S. Ma, Determining a random Schrödinger operator: Both potential and source are random, *Comm. Math. Phys.*, **381** (2021), 527–556.
[18] J. Li, H. Liu and S. Ma, Determining a random Schrödinger equation with unknown source and potential, *SIAM J. Math. Anal.*, **51** (2019), 3465–3491.
[19] R.-E. Plessix, A review of the adjoint-state method for computing the gradient of a functional with geophysical applications, *Geophysical Journal International*, **167** (2006), 495–503.
[20] R. A. Ponram, B. H. Prasad and S. S. Kumar, Thickness mapping of rocket motor casing using ultrasonic thickness gauge, *Materials Today: Proceedings*, **5** (2018), 11371–11375.
[21] M. J. D. Powell, Restart procedures for the conjugate gradient method, *Math. Programming*, **12** (1977), 241–254.
[22] W. Sun and Y.-X. Yuan, *Optimization Theory and Methods*, Nonlinear Programming, Springer, New York, 2006.
[23] D. Wei, Y.-A. Shi, B.-N. Shou, Y.-W. Gui, Y.-X. Du and G.-M. Xiao, Reconstruction of internal temperature distributions in heat materials by ultrasonic measurements, *Applied Thermal Engineering,* **112** (2017), 38–44.
[24] D. Wei, X. Yang, Y. Shi, G. Xiao, Y. Du and Y. Gui, A method for reconstructing two-dimensional surface and internal temperature distributions in structures by ultrasonic measurements, *Renewable Energy*, **150** (2020), 1108–1117.
[25] Y.-X. Yuan, Analysis on the conjugate gradient method, *Optimization Methods and Software*, **2** (1993), 19–29.

Received December 2020; 1st revision January 2021; 2nd revision February 2021.

E-mail address: youjundeng@csu.edu.cn, dengyijun_001@163.com
E-mail address: hongyu.liuip@gmail.com, hongyliu@cityu.edu.hk
E-mail address: xcwang90@gmail.com
E-mail address: xisuzisi@126.com
E-mail address: mtah_zly@163.com